PAPER

Check for updates

Bio-elastomer nanocomposites reinforced with surface-modified graphene oxide prepared *via in situ* coordination polymerization†

Arely Bahena,[a] Ilse Magaña,[a] Héctor Ricardo López González,[a] Rishab Handa,[b] Francisco Javier Enríquez-Medrano,[a] Sugam Kumar,[c] Ricardo Mendoza Carrizales,[a] Salvador Fernandez,*[a] Luis Valencia ⬡*[d] and Ramón Enrique Díaz de León Gómez*[a]

This article proposes a method to produce bio-elastomer nanocomposites, based on polyfarnesene or polymyrcene, reinforced with surface-modified graphene oxide (GO). The surface modification is performed by grafting alkylamines (octyl-, dodecyl-, and hexadecylamine) onto the surface of GO. The successful grafting was confirmed *via* spectroscopic (FTIR and Raman) and X-ray diffraction techniques. The estimated grafted amines appear to be around 30 wt%, as calculated *via* thermogravimetric analysis, increasing the inter-planar spacing among the nanosheets as a function of alkyl length in the amine. The resulting modified GOs were then used to prepare bio-elastomer nanocomposites *via in situ* coordination polymerization (using a ternary neodymium-based catalytic system), acting as reinforcing additives of polymyrcene and polyfarnesene. We demonstrated that the presence of the modified GO does not affect significantly the catalytic activity, nor the microstructure-control of the catalyst, which led to high *cis*-1,4 content bio-elastomers (>95%). Moreover, we show *via* rheometry that the presence of the modified-GO expands the capacity of the elastomer to store deformation or applied stress, as well as exhibit an activation energy an order of magnitude higher.

Introduction

The alarming environmental issues that we are currently facing demand the development of more eco-friendly materials that can gradually replace (non-renewable) petroleum-based ones. Most of the current industrially used rubbers are composed of butadiene or isoprene monomers, which are extracted by the steam cracking process of fossil fuel materials. Therefore, during the last decade, the development of bio-elastomers has been a great deal of research effort, aiming to produce elastomeric materials with competitive performance. A key alternative for this purpose is the use of bio-based terpenes.

Terpenes are unsaturated hydrocarbons that share the same polymerizable unit of isoprene monomer, a hemiterpene moiety.[1] The presence of a hemiterpene unit makes feasible the polymerization of most terpenes, including the non-

conventional ones such as β-myrcene, *trans*-β-farnesene, and β-ocimene, which could potentially yield polymers with similar rubbery features to polybutadiene (PB) and polyisoprene (PI).[2–4] Although β-myrcene and β-farnesene have readily proved their capacity to be polymerized,[4–6] the synthesis of these poly-terpenes with high performance, require control in their microstructure, which can be achieved *via* coordination polymerization. In this context, neodymium (Nd)-based catalytic system has demonstrated to give excellent results, yielding polydienes with a high content of *cis*-1,4 microstructure.[7,8]

A way to further enhance the performance of such elastomeric polymers is through the incorporation of graphitic nanofillers into the polymer matrix, to yield bio-elastomer nanocomposites with superior mechanical, electrical, and/or thermal behavior.[9–12] In the case of graphene oxide, which is a rather economical (though non-conductive) alternative of graphene, a major problem as nanofiller is the lack of interfacial bonding with the polymer matrix (due to its high hydrophilicity), therefore leading to poor dispersion and agglomeration of the nanosheets.[13–15] Nevertheless, GO has a vast amount of reactive functional groups, such as hydroxyl, epoxy, and carbonyl groups,[16–20] which provide reactive sites for surface modifying the nanosheets to tailor specific properties, such as enhancing their compatibility with polymer matrices.[15,21]

Even though different surface modification techniques in GO have been previously explored,[22–25] in this work we take

[a]*Research Center for Applied Chemistry, Blvd. Enrique Reyna 140, San José de los Cerritos, 25294, Saltillo, Coahuila, Mexico. E-mail: salvador.fernandez@ciqa.edu.mx; ramon.diazdeleon@ciqa.edu.mx*

[b]*Experimental Physics, Saarland University, 66123, Saarbrücken, Germany*

[c]*Solid State Physics Divison, Bhaba Atomic Research Centre, Mumbai, 400 085, India*

[d]*Materials Technology and Chemistry, Alfa Laval Tumba AB, SE-14782 Tumba, Sweden. E-mail: luisalexandro.valencialopez@alfalaval.com*

advantage of the high reactivity of alkylamines to modify the surface of GO. Alkylamines can strongly interact with the epoxy groups of GO via nucleophilic interactions,[26,27] and with the carbonyl groups via electrostatic interactions. On the other hand, in situ polymerization was selected as a suitable strategy to prepare the nanocomposites, as a good dispersion of GO nanosheets in polymer matrices has been previously observed via this method.[28,29] In this article, we report (i) the surface modification of GO with alkylamines of different alkyl lengths, (ii) the preparation of elastomeric nanocomposites based on polymyrcene (PM) and polyfarnesene (PF), reinforced with alkylamine modified-GO (hereinafter also referred as m-GO), via in situ coordination polymerization, using a ternary neodymium-based catalytic system. The successful surface modification of GO was confirmed via FTIR and Raman spectroscopy, as well as X-ray diffraction. Moreover, we estimated the amount of grafted alkylamines via thermogravimetric analyses. Then, we studied the influence of various loadings of m-GO over the properties of PF and PM, focusing specifically on the microstructure, molecular weight characteristics, and viscoelastic properties.

Experimental part

Materials

Graphite flakes (carbon 99%), sulfuric acid (H_2SO_4), and hydrochloric acid (HCl) were supplied from Sigma Aldrich. Hydrogen peroxide (H_2O_2) was supplied from JT Baker, potassium permanganate ($KMnO_4$) was supplied from Fermont and the alkylamines (octylamine, dodecylamine, and hexadecylamine) were purchased from Tokyo Chemical Industry Co., Ltd. The monomers β-myrcene (Ventos, purity >85%) and trans-β-farnesene (Amyris purity ~100%) were distilled from sodium under vacuum before use. The catalyst neodymium versatate (NdV_3, 0.5 M solution in hexane) was obtained from SOLVAY and it was used as received. The co-catalyst diisobutylaluminum hydride (DIBAH, 1.0 M solution in hexane) and dimethyldichlorosilane (DMDCS, ≥99.5%) were acquired from Sigma Aldrich. Cyclohexane (Reagent grade, Sigma Aldrich) was twice distilled from sodium under argon atmosphere before use.

Methods

GO synthesis. GO was prepared from exfoliated graphite flakes via the modified Hummers method.[30] First, a mixture of concentrated H_2SO_4 (250 mL) and $KMnO_4$ (30 g) was stirred in a 1 L Erlenmeyer flask for 5 minutes at room temperature. Then, the exfoliated graphite flakes (10 g) were added into the mixture and dispersed for 30 minutes in an ultrasound bath at 35 °C. The mixture was then transferred to a 2 L beaker containing distilled water (500 mL) and stirred thoroughly for 10 minutes. An H_2O_2 aq. solution 30% (v/v) was then added slowly until the effervescence was over (~30 mL) and stirred for further 10 minutes and distilled water was then added (until reaching a volume of approximately 1.8 L). The mixture was sedimented, yielding a light brown solid, which was subsequently separated by decantation. The solid was repeatedly washed with

a concentrated HCl solution, sedimented by centrifugation and decantation until reaching a neutral pH. Finally, the dried solid was obtained by lyophilization. TEM micrographs of the synthesized GO, displaying the size and morphology, are presented in the ESI.

Surface modification of GO with alkylamines. 2 g of GO and 200 mL of a 70/30% (v/v) ethanol/water solvent mixture were added to a 500 mL flask, and homogenously dispersed via sonication: 30 minutes immersed in an ultrasound bath, the solution was then sonicated with a tip sonicator for 5 minutes at 60% amplitude. Then, 18 mmol of alkylamine (octylamine, dodecylamine, or hexadecylamine) were added and the sonication continued for an additional 5 minutes. The purification of m-GO was carried out by centrifugation, using a 70/30% (v/v) ethanol/hot water solution. The decanted solid was filtered and then washed with hot ethanol and acetone. The resultant material was dried for 12 hours at 70 °C in a vacuum oven. The m-GO was then ground in a planetary mill for 25 minutes where 25 mL of cyclohexane per gram of m-GO was added. Finally, it was transferred to a 100 mL vial, under a nitrogen atmosphere, prior polymerization.

In situ polymerization of β-myrcene and trans-β-farnesene. All manipulations for the preparation of polymerization reactions were carried out under inert atmosphere in an MBraun glove box. The catalytic system was prepared as follows: the components were added into a glass vial under nitrogen atmosphere in the following order of addition: (i) DIBAH (co-catalyst), (ii) NdV_3 (catalyst), and (iii) DMDCS (halide donor) in a NdV_3/DIBAH/DMDCS molar ratio of 1/25/1, respectively. Then, they were aged (under mild stirring) for 30 minutes. The in situ polymerization reactions were carried out in 100 mL glass vials under nitrogen atmosphere. For the reactions, 70 mL of cyclohexane and 10 g of monomer (β-myrcene or trans-β-farnesene) were added to the vial. Then, the vial was placed in an oil bath and heated up to 60 °C. The GO suspension (of variable concentration, explained later in the manuscript) was then added, followed by the addition of the pre-aged catalytic system (5 minutes after adding the GO). The deactivation of the reaction was performed by adding a small amount of acidified methanol with Irganox 1076 (0.5 wt%). Finally, the polymer was precipitated with methanol and vacuum dried at room temperature. GO completely remains in the elastomeric matrix.

Characterization

Modified graphene oxide. The chemical composition of the m-GO samples was analyzed by Fourier-transform infrared-spectroscopy (FTIR) using a Thermo Scientific Nicolet iS 5 FT-IR spectrometer with a germanium crystal. The spectra were the result of 32-times averaged scans and were acquired at a resolution of 4 cm^{-1}. Raman spectroscopy was carried out using a MicroRaman Horiba XploRA in a frequency range of 3000 to 200 min^{-1}, using a 532 nm laser. The powder X-ray diffractograms (PXRD) were obtained using a Bruker D8Advance ECO. The radiation frequency was the Cu line Kα1 (wavelength (λ) = 1.5418 Å). The settings are current of 40 mA and tension of 45 kV with a step size of 0.05 at room

temperature. The thermal behavior was studied by thermogravimetric analysis (TGA) using a TA-Q500 from TA Instruments, heating the samples from 30–600 °C at a constant heating rate of 10 K min^{-1} under a nitrogen flow of 50 mL min^{-1}.

Polymer nanocomposites. The molecular weight characteristics of the polymers were determined by size exclusion chromatography (SEC) using an Agilent Technologies model PL-GPC 50, configured with a 5 μm mixed type column at a pressure of 2.34 MPa and refraction index detector calibrated with polystyrene standards. Polymer samples were dissolved in THF in a weight:volume ratio (1 : 1). The chemical microstructure of the elastomers (PM and PF) was determined by ^{1}H and ^{13}C nuclear magnetic resonance (NMR) using a Bruker Ultrashield Plus 500 MHz spectrometer. Deuterated chloroform (CDCl$_3$) was used as the solvent and the analyses were performed at room temperature, 16 scans for the ^{1}H, and 15 000 scans for the ^{13}C NMR measurements. Differential Scanning Calorimetry (DSC) thermograms were obtained using a TA Instruments DSC 2920. The analyses were carried out under nitrogen atmosphere and at a heating rate of 5 °C min^{-1}. The rheological measurements were carried out using an Anton Parr Q300 rheometer in plate/plate configuration with a diameter of 25 mm. Frequency sweep protocol was used with constant deformation of 5% at 0.001 to 300 Hz. The samples were analyzed at 23, 50, 90, and 120 °C.

Results and discussion

Surface modification of GO with alkylamines

Intending to improve the compatibility between GO and polyterpene matrices, we modified the surface of GO by incorporation of alkylamines, which can interact chemically and physically with the epoxy and carboxyl groups of GO, respectively (see Fig. 1). Three different alkylamines (with different alky length) were used for this study, octylamine, dodecylamine, and hexadecylamine, yielding three types of m-GO's: GO$_{oct}$, GO$_{dod}$, and GO$_{hex}$, respectively. A conceptual schematic diagram of the surface modification of GO is shown in Fig. 1.

The surface modification of the GO nanosheets with the different alkylamines was first confirmed by analyzing their chemical composition *via* FTIR spectroscopy (see Fig. 2a). All spectra displayed the characteristic bands of GO at 1730, 1620,
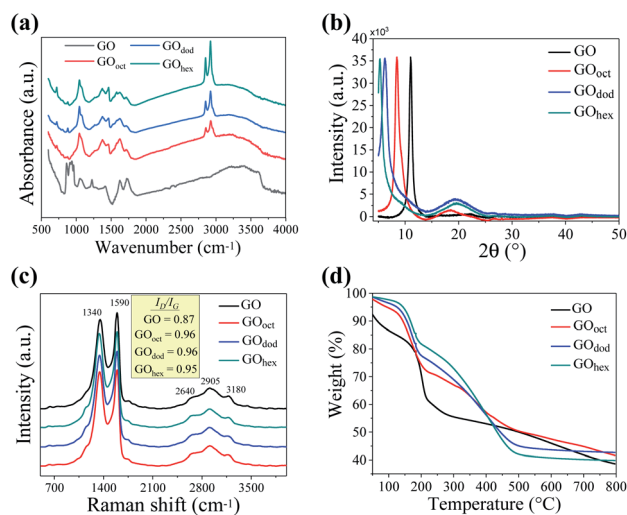

Fig. 2 Physicochemical characterization of GO and m-GO's (a) FTIR spectra; (b) PXRD patterns; (c) Raman spectra, and (d) TGA thermogram of GO and m-GO's. The intensities of FTIR, Raman, and XRD spectra were normalized for a proper comparison.

1220, and 1050 cm^{-1} which correspond to the C=O stretching vibrations, stretching of the intercalated water molecules, C–O stretching of the epoxide groups, and C–O stretching of alkoxy groups, respectively.[31,32] In the spectra corresponding to the m-GO's, two further asymmetric bands can be appreciated at 2920 and 2850 cm^{-1} in all cases, which indeed correspond to the stretching vibrations of the C–H bond from the incorporated alkylamines.[27,33,34] Higher peak intensity was observed as a function of the length of the alkyl chain. The bands located at 1590 and 1450 cm^{-1}, on the other hand, correspond to the deformation vibrations of the N–H bond and the formation of C–N bands,[26] demonstrating the successful grafting of the alkylamines in the GO structure. It was furthermore observed that, in all cases, the signal corresponding to the epoxide group (≈ 1220 cm^{-1}) disappears completely. This fact confirms the nucleophilic ring-opening reaction of the epoxy groups in the presence of the alkylamines.

The diffraction patterns, obtained by PXRD, are shown in Fig. 2b. The representative crystalline peak of GO was observed at 11°, as opposed to the one observed for graphite around 25°, demonstrating the increase of the laminar spacing between the
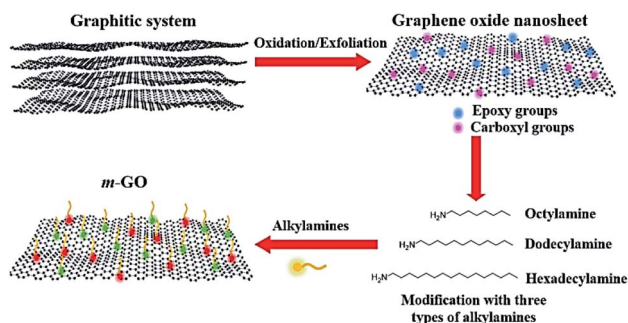

Fig. 1 Conceptual schematic illustration of the process followed for the modification of GO with different alkylamines.

Table 1 Variation in the GO and m-GO's inter-sheet spacing

Sample	Peak position $2\theta_p$ (°)	Inter-planar spacing (Å)	δ^a (Å)	Crystallite size τ (Å)
GO	11	8.03	—	125.0
GO$_{oct}$	8.4	10.56	11.62	88.2
GO$_{dod}$	6.3	14.02	16.68	58.0
GO$_{hex}$	5.3	16.75	21.74	—

^{a} Extended tail length of alkyl chain as calculated by Tanford's equation $[\delta = (1.5 + 1.265n_C)]$, where n_C denotes the number of carbon atoms in the tail.

nanosheets.[35,36] In the case of the m-GO's, a shift of the diffraction peak towards even lower angles was observed, which indeed decreased as a function of alkyl chain length (GO$_{oct}$ at 8.4°, GO$_{dod}$ at 6.3°, and GO$_{hex}$ at 5.3°) clearly suggesting a larger inter-layer spacing upon modification with longer alkylamine chains. The variation in the inter-planar spacing as calculated using Bragg's law is depicted in Table 1. It may be mentioned here that the increase in the inter-planar spacing on the addition of alkylamines is much smaller than the extended alkyl chain lengths, suggesting that the alkylamine chains are neither fully extended nor oriented in the perpendicular direction between the GO nanosheets. The crystallite size (τ) as calculated employing Scherrer formula [$\tau = K\lambda/\beta \cos \theta_p$], where K ($\sim$9) is a dimensionless shape factor, θ_p is half of the scattering angle at peak position, and β is the line broadening at FWHM. The values have also been presented in Table 1. As it can be observed, the crystallite size decreases with increasing chain length, probably because of the structural disruption caused by the grafting of the alkyl chains. However, the peak for the GO$_{hex}$ samples appears to be sharper compare to those observed for the GO$_{oct}$ and GO$_{dod}$ samples, but we could not calculate the crystallite size for this sample as the full peak was not observed in the measured scattering angle range.

The appearance of a low-intensity halo was observed $\approx$20° in the case of the m-GO's, which is attributed to the presence of stacked sheets of graphene with a low degree of oxidation.[23] This behavior suggests a partial reduction of GO upon the incorporation of alkylamines, apparently promoted by longer alkyl chains in the alkylamines.

Further characterization of the m-GO's was carried out by Raman spectroscopy. Raman provides valuable information regarding various properties of carbon nanomaterials (such as defects, crystallite size, and number of layers), considering that conjugated and double carbon–carbon bonds lead to important Raman intensities.[37] The Raman spectra of all samples (shown in Fig. 2c) exhibit two main high-intensity bands, the in-phase vibration of the graphite lattice (G band) around 1550 cm^{-1} and the disorder band caused by the graphitic edges (D band) around 1350 cm^{-1} (band G).[37,38] Moreover, a broad signal between 2500 to 3500 cm^{-1}, the 2D band, was furthermore observed, which is composed of the characteristic signal at 2640 cm^{-1} that reveals the presence of a low number of stacked layers of graphene, as previously observed by XRD.[39]

It is known that graphite shows the near absence of the Raman D band, as symmetry-breaking of the graphene edges is required to be Raman visible;[37] therefore, our results in Fig. 2c corroborate the formation of GO as a prominent D band is observed. In addition, typical G bands in graphite are shown as narrow peaks, whilst our spectra display broad bands in all samples, implying a high degree of disorder, as expected for GO and the obtained modified derivatives.

An increase in the I_D/I_G ratio was observed upon modification of GO with the alkylamines, which indeed suggests the cleavage of sp^2 bonds and the creation of sp^3 ones, i.e., introducing structural defects.

The thermal stability of GO and m-GO's, before and after modification, was studied by TGA, the results are shown in
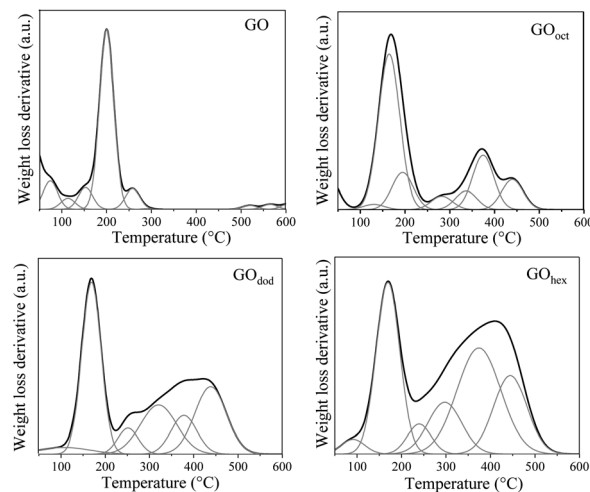

Fig. 3 Deconvoluted weight-loss derivatives as a function of temperature (determined by TGA) of GO and m-GO's.

Fig. 2d. A first mass-loss was observed in all samples around 100 °C, attributed to moisture loss. The degradation at this temperature was significantly lower for all m-GO's, proving their lower water-uptake and hydrophobicity upon modification, which is a required property to enhance their compatibility with the polymer matrices. The mass-loss around 185 °C, on the other hand, corresponds to the release of CO and CO$_2$ resulting from the presence of functional groups that contain labile oxygen, observed in all samples. Moreover, the thermograms of all the m-GO's show an evident difference to the pristine GO at higher temperatures. For instance, pristine GO exhibits a single degradation onset around 200 °C, whereas the m-GO's samples clearly show a secondary degradation step around 300 °C. This behavior can be elucidated by looking at the weight loss derivative as a function of temperature, which can be deconvoluted in multiple Gaussian functions (Fig. 3). By estimating the %-area of the distributions above 300 °C (which are not observed in pristine GO), we can get an approximate quantification of the grafted alkylamines onto the m-GO's, which correspond to 33.8, 34, and 35.3 wt% of the corresponding alkylamines in GO$_{oct}$, GO$_{dod}$, and GO$_{hex}$, respectively. These
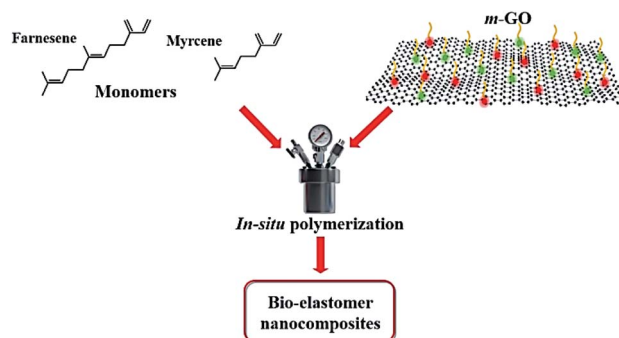

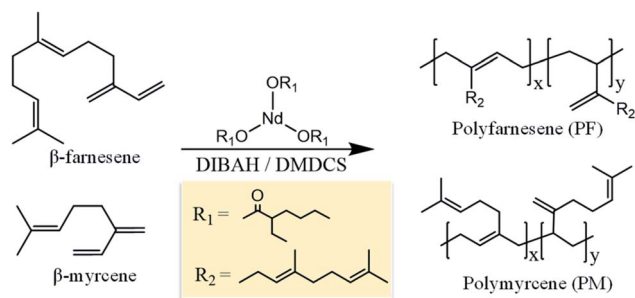Fig. 4 Schematic illustration of the synthesis of bio-elastomeric nanocomposites.

Fig. 5 Schematic representation of the polymerization of β-myrcene and *trans*-β-farnesene using the catalytic system comprising NdV₃, DIBAH (co-catalyst), and DMDCS (halide donor).

values suggest a quasi-equal reactivity among GO and the different alkylamines, whereas the small weigh-difference is due to the alkyl chain length discrepancy.

Synthesis of the elastomeric nanocomposites based on polyfarnese and polymyrcene

The different grades of m-GO's were furthermore incorporated into PM and PF matrices *via in situ* polymerization (see Fig. 4), yielding bio-elastomeric nanocomposites (referred as PM/m-GO or PF/m-GO, respectively). *In situ* polymerization here refers to polymerize the monomers in the presence of the graphitic filler (pre-dispersed in the reaction medium), which was herein carried out *via* coordination polymerization using the catalytic system comprising NdV₃ (catalyst), DIBAH (co-catalyst), and DMDCS (halide donor) (see Fig. 5). This type of polymerization offers the possibility to control the microstructure of terpenes, *i.e.*, their isomerism, which is indeed required to produce high-performance rubbers. Nevertheless, the employed catalytic system is overly sensitive to deactivation, and therefore it is not intuitive to know how the incorporated fillers will affect the polymerization behavior.

NdV₃, a rare earth metal-based catalyst, has been previously reported for its efficiency to polymerize terpenes, as well as good control in stereospecificity and molecular weight characteristics.[40–42] NdV₃ is commonly combined with alkylaluminiums (here DIBAH), which act as co-catalysts, *i.e.*, acting as acid Lewis abstracting alkyl groups from the metal and create free-coordination sites, forming the catalytic species. Halide donors (here DMDCS) are also included in the catalytic system to generate the active species for the polymerization and to enhance the microstructure-control by coordinating the Nd atom and thus promoting the *cis* coordination of terpenes. A schematic representation of the catalytic system used to polymerize β-myrcene and *trans*-β-farnesene is shown in Fig. 5.

Effect of the surface modification of GO over the polymerization behaviour. A series of polymerization reactions were performed in the presence of GO and the different m-GO alkylamine derivatives (GO$_{oct}$, GO$_{dod}$, and GO$_{hex}$) at a constant filler loading (0.5 wt%) and equal reaction parameters. The results are summarized in Table 2. The catalytic activity was rather constant regardless of the surface modification of GO, achieving almost full conversion in all cases. In the synthesis of PF nanocomposites, it is evident that the presence of either GO or m-GO does not significantly affect the catalytic activity or the yield in the polymerization reactions. However, there are important changes in the molecular weight characteristics (M_w and $Đ$) of the synthesized polymers (Table 2). These discrepancies can be attributed to a deactivation process of the catalytic species during the polymerization reaction.

The behavior in the synthesis of PM nanocomposite, on the other hand, is different. The presence of the different m-GO's or GO, and specifically the type of surface modification, has a direct effect over the activity of the catalytic system and the yield of the polymerization reactions. This phenomenon was attributed to a deactivation process with respect to time, which unlike the synthesis of PF nanocomposites, is apparently favored by the lower steric volume of the β-myrcene monomer. This fact suggests that the greater steric volume of the *trans*-β-

Table 2 Effect of the incorporation of GO and m-GO in the polymerization of β-myrcene and *trans*-β-farnesene. (0.5 wt% of filler was used in all samples)[a]

Run	Filler	Yield[b] (%)	A^c	M_w (kDa)	$Đ^d$	T_g^e (°C)	1,4-content[f] (%)	1,4-cis[g] (%)
PF-1	—	100	123	93	2.8	−73.8	96.1	N.D.
PF-2	GO	100	123	710	4.7	−74.5	99.6	N.D.
PF-3	GO$_{oct}$	100	123	84	3.9	−74.2	98.6	N.D.
PF-4	GO$_{dod}$	98	120	689	7.4	−73.6	99.6	N.D.
PF-5	GO$_{hex}$	96	118	180	4	−71.4	95.8	N.D.
PM-1	—	97	215	303	4.1	−64.7	97.1	96
PM-2	GO	96	213	299	4	−65.2	97.0	92
PM-3	GO$_{oct}$	94	180	470	4.7	−64.4	97.1	93
PM-4	GO$_{dod}$	94	123	1800	3.7	−63.9	98.0	94
PM-5	GO$_{hex}$	90	161	361	4.2	−64.7	96.9	95

[a] All reactions were performed in cyclohexane at 60 °C. The catalytic system used was NdV₃/DIBAH/DMDCS. N.D. = not determined. *Trans*-β-farnesene reactions were carried out using a monomer/Nd molar ratio of 300 and the total reaction time was 60 minutes. β-Myrcene reactions were carried out using a monomer/Nd molar ratio of 1000 and the total reaction time was 90 minutes. [b] Final reaction yield percentage calculated by gravimetry. [c] Catalytic activity calculated after 30 min of reaction (kg$_{polymer}$/mol$_{Nd}$ h). [d] Dispersity (M_w/M_n) determined by SEC. [e] Determined by DSC. [f] Calculated from the ¹H NMR spectra. [g] Calculated from the ¹³C NMR spectra.

farnesene monomer prevents this deactivation process with respect to time. Interestingly, the presence of m-GO or GO does not affect the coordination mechanism of both monomers, as demonstrated by the quasi-constant values of 1,4 microstructure (see Table 2). The *cis*-1,4 microstructure values determined in the synthesized PM nanocomposites are between 92–96%.

These results demonstrate the excellent microstructure-control provided by the catalytic system over the bio-terpene polymerization, which is not affected by the incorporation of the nanofillers. The T_g of the polymers was found between −71 and −75 °C for PF and between −63 and −65 °C for PM, which is within the range already reported in the literature.[43,44] The T_g corresponding to PF-1 and PMy-1, both without GO, was slightly lower than those having GO at 0.5 wt% (PF-2 and PMy-2), which is attributed to the restriction of the polymer chain mobility due the presence of GO which presumably constrains the molecular relaxation and thus promoting an increase in the T_g.[45,46] On the other hand, when m-GO was used instead of GO, the T_g of the polyterpenes tends to decrease. The m-GO seems to reduce the cohesive forces through the polymer chains (acting as plasticizer), causing a decrease in T_g.

To elucidate the influence of the different m-GO's over the mechanical response of the polyterpenes (using solely PF as a model system), we carried out a series of rheological measurements, using a stress-controlled rheometer in plate/plate configuration (under nitrogen atmosphere to avoid crosslinking during the measurements). We measured the linear viscoelastic moduli $G'(\omega)$ and $G''(\omega)$ in frequency sweep, and the results are summarized in Fig. 6 along with the corresponding viscosity of the PF/m-GO nanocomposites.

A power-law dependence of G' and G'' on the frequency for all the samples indicate typical microstructural relaxation for elastomers. Surprisingly, all PF/m-GO nanocomposites, compared to pristine PF, exhibit $G' > G''$, scaling as $G' \sim \omega^{1/3}$, which corresponds to a highly elastic response. Whereas the bulk of material remains stiff, as G'' is constant in the rubbery plateau presumably due to restricted movement and rearrangements of the PF segments condensed by the strong

interfacial ionic interaction with the m-GO's (reduced free volume effect). This behavior suggests that the incorporation of the m-GO in PF significantly expands the capacity of the elastomer to store deformation or applied stress with additional contribution from enthalpic interactions of soft cross-linked segmental stretching.[47] In addition, PF-1 and PF-4 showed a shear-thinning behavior, however, with a difference of approximately 3 orders of magnitude (see Fig. 6(a) inset). This jump in viscosity of PF reinforced with GO_{dod} favorably support our prospect of introducing bio-elastomers with enhanced rheological features and performance.

On the other hand, a significant difference between PF and the PF/m-GO nanocomposites is obtained for the viscosity η as a function of inverse temperature (see Fig. 6(b)). The Arrhenius dependence of η for PF reveals the activation energy of $E_a \approx 1.3 \pm 0.2$ kJ mol^{-1}. Nevertheless, the PF/m-GO show an order of magnitude higher activation energy with $E_a \approx 90 \pm 5$ kJ mol^{-1}, which is found in a close agreement with E_a values reported for silicone rubbers.[47,48] Note that we relate our values of E_a to the viscous dissipation of the PF-GO composite and not the thermo-oxidative processes and hemolytic dissociation of crosslinked bridges between PF and GO as reported otherwise.[49] Comparing the rheological response of our PF/m-GO samples to petroleum-based elastomers, such as styrene-butadiene rubbers and hyperbranched polyisoprene, our values of G' over the corresponding unshifted frequency range and η are found in a good agreement to the studies,[47,50,51] reporting shear thinning behavior and strong elastic response as shown in Fig. 6. Note that, the performance of rubbers entirely depends also on the curing system (vulcanization), and therefore, we cannot really compare the performance of our bio-elastomers with commercial rubbers. Conclusively, our modified PF/m-GO does compete with on par mechanical performance for prospective applications, and opens up eco-friendly opportunities to further improve the pathways to synthesize bio-elastomers with relatively rich mechanical and thermal features, primarily by utilizing the stereospecific nature of farnesene-like monomers.

Effect of the content of m-GO over the polymerization of β-farnesene and β-myrcene. To further understand the influence of the m-GO over the polyterpenes' properties, a series of reactions were carried out, introducing different loadings (0, 0.10, 0.25, 0.50, 0.75, and 1.0 wt%) of dodecyl-modified GO (GO_{dod}). This material was selected as a model system simply because it is a middle point among the three types of alkylamines. The results are summarized in Table 3.

In the synthesis of PF nanocomposites, it was evident that the presence of GO_{dod} does not significantly affect the catalytic activity of the catalyst system, independently of the loaded amount. Nevertheless, the molecular weight appears to increase non-monotonically as a function of loaded m-GO. This behavior suggests a partial deactivation of the catalytic species. At difference of the synthesis of PF nanocomposites, the catalytic activity and yield in the synthesis of PM nanocomposites, with different loadings of GO_{dod}, were affected significantly when the presence of GO_{dod} was higher ≥0.75 wt%. This phenomenon is, as already mentioned before in the manuscript, is presumably favored by the lower steric volume of the β-myrcene monomer,
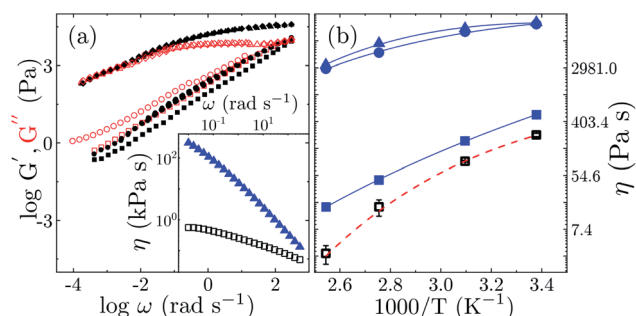

Fig. 6 (a) Viscoelastic moduli G' (solid symbols) and G'' (open symbols) are depicted as a function of frequency ω. Inset: logarithmic representation of frequency dependence of the viscosity of PF-1 and PF-4. (b) Arrhenius fit of viscous response of PF (open symbols) and PF-GO composites (solid symbols) for η taken at $\omega \sim 1$ rad s^{-1}. Legends; squares: PF (PF-1), circles: PF/GO_{oct} (PF-3), triangles: PF/GO_{dod} (PF-4), and diamonds: PF/GO_{hex} (PF-5).

Table 3 Effect of variation of GO_{dod} content in the *in situ* polymerization of β-myrcene and *trans*-β-farnesene[a]

Run	GO_{dod} (wt%)	Yield[b] (%)	A^c	M_w (kDa)	$Đ^d$	T_g^e (°C)
PF-1	—	100	123	93	2.8	−73.8
PF-6	0.10	100	121	160	5.2	−75.1
PF-7	0.25	100	120	475	10.2	−73.8
PF-4	0.50	98	120	689	7.4	−73.6
PF-8	0.75	100	119	532	9.1	−73.1
PF-9	1.00	94	112	1220	5.1	−71.4
PM-1	—	97	215	303	4.1	−64.7
PM-6	0.10	95	180	334	4	−65.7
PM-7	0.25	90	147	301	4.2	−65.1
PM-4	0.50	94	123	1800	3.7	−63.9
PM-8	0.75	93	131	354	5.7	−64.4
PM-9	1.00	88	117	1251	4.8	−64.7

[a] All reactions were performed in cyclohexane at 60 °C. The catalyst system used was NdV_3, DIBAH, and DMDCS. PF reactions were carried out using a monomer/Nd molar ratio of 300 with a total reaction time of 60 minutes. PM reactions were carried out using a monomer/Nd molar ratio of 1000 with a total reaction time of 90 minutes. [b] Final reaction yield percentage calculated by gravimetry. [c] Catalytic activity determined after 30 min of reaction ($kg_{polymer}$/ mol_{Nd} h). [d] Dispersity (M_w/M_n) determined by SEC. [e] Determined by DSC.

which presumably promotes in greater extent the deactivation process of the catalytic species.

Conclusions

In this work, we demonstrate a straightforward method to produce bio-elastomer nanocomposites, based on poly-farnesene or polymyrcene, reinforced with surface-modified GO. Alkylamines, with different alkyl length, can be grafted onto the surface of GO, which interacts *via* a nucleophilic ring-opening reaction with the epoxy groups of GO (as demonstrated by FTIR), as well as *via* electrostatic interactions with the carbonyl groups. The estimated grafted amines appear to be around 30 wt%, as calculated by thermogravimetric analysis. The presence of alkylamines increases the inter-planar spacing among the GO nanosheets as a function of alkyl length chain, as proved by PXRD, whilst decreasing the crystallite size, presumably due to the structural defects which are introduced during the surface-modification, as also corroborated by Raman spectroscopy.

The resulting modified-GO's were then used to prepare bio-elastomer nanocomposites *via in situ* coordination polymerization using NdV_3/DIBAH/DMDCS as a catalyst system. We demonstrated that the presence of the modified-GO does not significantly affect the catalytic activity, nor microstructure control of the catalyst, which led to high *cis*-1,4 (>95%) content bio-elastomers, with a T_g around 74 °C and 64 °C for poly-farnesene and polymyrcene, respectively. We furthermore proved, *via* rheometry, that the presence of the modified-GO expands the capacity of the elastomer to store deformation or applied stress, as well as increasing the activation energy an order of magnitude higher. Our results provide relevant insights

towards the synthesis of sustainable alternatives for elastomers, which can potentially replace petroleum-based materials in the upcoming future.

Conflicts of interest

There are no conflicts to declare.

Acknowledgements

References

1 P. A. Wilbon, F. Chu and C. Tang, *Macromol. Rapid Commun.*, 2013, **34**, 32–43.

2 J. M. Bolton, M. A. Hillmyer and T. R. Hoye, *ACS Macro Lett.*, 2014, **3**, 717–720.

3 P. Sahu, P. Sarkar and A. K. Bhowmick, *ACS Sustainable Chem. Eng.*, 2017, **5**, 7659–7669.

4 A. Behr and L. Johnen, *ChemSusChem*, 2009, **2**, 1072–1095.

5 T. Yoo and S. K. Henning, *Rubber Chem. Technol.*, 2017, **90**, 308–324.

6 C. Iacob, T. Yoo and J. Runt, *Macromolecules*, 2018, **51**, 4917–4922.

7 L. Friebe, O. Nuyken, H. Windisch and W. Obrecht, *Macromol. Chem. Phys.*, 2002, **203**, 1055–1064.

8 Y. Hu, C. Zhang, X. Liu, K. Gao, Y. Cao, C. Zhang and X. Zhang, *J. Appl. Polym. Sci.*, 2014, **131**, 40153.

9 S. Araby, Q. Meng, L. Zhang, I. Zaman, P. Majewski and J. Ma, *Nanotechnology*, 2015, **26**, 112001.

10 J. R. Potts, O. Shankar, L. Du and R. S. Ruoff, *Macromolecules*, 2012, **45**, 6045–6055.

11 S. H. Song, O. S. Kwon, H. K. Jeong and Y. G. Kang, *Korean J. Mater. Res.*, 2010, **20**, 104–110.

12 D. G. Papageorgiou, I. A. Kinloch and R. J. Young, *Carbon*, 2015, **95**, 460–484.

13 J. Jang, V. H. Pham, S. H. Hur and J. S. Chung, *J. Colloid Interface Sci.*, 2014, **424**, 62–66.

14 B. Dehghanzad, M. K. Razavi Aghjeh, O. Rafeie, A. Tavakoli and A. Jameie Oskooie, *RSC Adv.*, 2016, **6**, 3578–3585.

15 X. Ji, Y. Xu, W. Zhang, L. Cui and J. Liu, *Composites, Part A*, 2016, **87**, 29–45.

16 S. Thampi, V. Muthuvijayan and R. Parameswaran, *RSC Adv.*, 2016, **6**, 104235–104245.

17 P. Karthika, N. Rajalakshmi and K. S. Dhathathreyan, *Soft Nanosci. Lett.*, 2012, **02**, 59–66.

18 J. L. Yan, G. J. Chen, J. Cao, W. Yang, B. H. Xie and M. B. Yang, *New Carbon Mater.*, 2012, **27**, 370–376.

19 F. Samadaei, M. Salami-Kalajahi, H. Roghani-Mamaqani and M. Banaei, *RSC Adv.*, 2015, **5**, 71835–71843.

RSC Advances

Paper

20 L. Valencia, S. Monti, S. Kumar, P. Liu, C. Zhu, S. Yu and A. Mathew, *Nanoscale*, 2019, **11**, 22413–22422.

21 S. Guo, Y. Nishina, A. Bianco and C. Ménard-Moyon, *Angew. Chem., Int. Ed.*, 2020, **59**, 1542–1547.

22 B. Zhang, L. Li, Z. Wang, S. Xie, Y. Zhang, Y. Shen, M. Yu, B. Deng, Q. Huang, C. Fan and J. Li, *J. Mater. Chem.*, 2012, **22**, 7775–7781.

23 N. A. Daud, B. W. Chieng, N. A. Ibrahim, Z. A. Talib, E. N. Muhamad and Z. Z. Abidin, *Nanomaterials*, 2017, **7**, 165.

24 S. Stankovich, R. D. Piner, S. B. T. Nguyen and R. S. Ruoff, *Carbon*, 2006, **44**, 3342–3347.

25 W. Li, X. Z. Tang, H. Bin Zhang, Z. G. Jiang, Z. Z. Yu, X. S. Du and Y. W. Mai, *Carbon*, 2011, **49**, 4724–4730.

26 A. B. Bourlinos, D. Gournis, D. Petridis, T. Szabó, A. Szeri and I. Dékány, *Langmuir*, 2003, **19**, 6050–6055.

27 A. M. Shanmugharaj, J. H. Yoon, W. J. Yang and S. H. Ryu, *J. Colloid Interface Sci.*, 2013, **401**, 148–154.

28 H. Kim, Y. Miura and C. W. MacOsko, *Chem. Mater.*, 2010, **22**, 3441–3450.

29 Y. Huang, Y. Qin, Y. Zhou, H. Niu, Z. Z. Yu and J. Y. Dong, *Chem. Mater.*, 2010, **22**, 4096–4102.

30 W. S. Hummers and R. E. Offeman, *J. Am. Chem. Soc.*, 1958, **80**, 1339.

31 J. H. Kang, T. Kim, J. Choi, J. Park, Y. S. Kim, M. S. Chang, H. Jung, K. T. Park, S. J. Yang and C. R. Park, *Chem. Mater.*, 2016, **28**, 756–764.

32 D. He, Z. Peng, W. Gong, Y. Luo, P. Zhao and L. Kong, *RSC Adv.*, 2015, **5**, 11966–11972.

33 X. Yang, T. Mei, J. Yang, C. Zhang, M. Lv and X. Wang, *Appl. Surf. Sci.*, 2014, **305**, 725–731.

34 A. M. Asiri, *Polym. Eng. Sci.*, 2012, **52**, 1212–1216.

35 F. T. Johra, J. W. Lee and W. G. Jung, *J. Ind. Eng. Chem.*, 2014, **20**, 2833–2887.

36 Y. Zhu, S. Murali, W. Cai, X. Li, J. W. Suk, J. R. Potts and R. S. Ruoff, *Adv. Mater.*, 2010, **22**, 3906–3924.

37 K. N. Kudin, B. Ozbas, H. C. Schniepp, R. K. Prud'homme, I. A. Aksay and R. Car, *Nano Lett.*, 2008, **8**, 36–41.

38 W. Gao, in *Graphene Oxide: Reduction Recipes, Spectroscopy, and Applications*, 2015, pp. 61–95.

39 A. Kaniyoor and S. Ramaprabhu, *AIP Adv.*, 2012, **2**, 032183.

40 D. Leon and Y. A. De Santiago-rodriguez, *Macromol. Symp.*, 2013, **325**, 125–131.

41 F. J. Enr, R. M. Carrizales, K. R. Acosta and M. Textle, *Can. J. Chem. Eng.*, 2016, **94**, 823–832.

42 R. D. De León, R. López, L. Valencia, R. Mendoza, J. Cabello and J. Enríquez, *Key Eng. Mater.*, 2018, **779**, 115–121.

43 P. Sarkar and A. K. Bhowmick, *RSC Adv.*, 2014, **4**, 61343–61354.

44 P. Sarkar and A. K. Bhowmick, *J. Appl. Polym. Sci.*, 2018, **135**, 45701.

45 B. Mensah, S. I. Kang, W. Wang and C. Nah, *Mech. Adv. Mater. Mod. Process.*, 2018, **4**, 1.

46 H. Akhina, K. A. Ramya, M. R. Gopinathan Nair, A. Saiter-Fourcin, M.-R. Garda, A. P. Deshpande, N. Kalarikkal and S. Thomas, *RSC Adv.*, 2020, **10**, 29247–29256.

47 M. M. Möwes, F. Fleck and M. Klüppel, *Rubber Chem. Technol.*, 2014, **87**, 70–85.

48 H. Ou, M. Sahli, T. Barriere and J.-C. Gelin, in *MATEC Web of Conferences*, 2016, vol. 80, p. 16007.

49 P. Rybiński and G. Janowska, *J. Therm. Anal. Calorim.*, 2014, **117**, 377–386.

50 S. Habibu, N. M. Sarih, N. A. Sairi and M. Zulkifli, *R. Soc. Open Sci.*, 2020, **6**, 190869.

51 A. Crié, C. Baritaud, R. Valette and B. Vergnes, *Polym. Eng. Sci.*, 2015, **55**, 2156–2162.